Fringe Tracking at the MROI

C.A. Jurgenson [a*], F.G. Santoro [a], F. Baron[b], K. McCord[a], E.K. Block[a], D.F. Buscher[b], C.A. Haniff[b], J.S. Young [b], T.A. Coleman[a], M.J. Creech-Eakman [a]

[a] New Mexico Institute of Mining and Technology, Magdalena Ridge Observatory, 801 Leroy Place, Socorro, NM 87801, USA;

[b] University of Cambridge, Cavendish Laboratory, Dept. of Physics, JJ Thomson Avenue, Cambridge, CB3 OHE, UK

ABSTRACT

We report on the opto-mechanical design of the MROI fringe tracker. This instrument, currently under development in collaboration with the University of Cambridge, will be a dedicated fringe tracking beam combiner and spectrographs. I will utilize the "Y" geometry of the array to stabilize fringes on shorter "nearest neighbor" baselines, and thus allow for increased integration times on the longer baselines and the buildup of signal to noise. The beam combiner has been designed to accommodate light from a maximum of ten telescopes (three in each array arm, one at the "Y" vertex), but can operate with fewer without having to change the overall layout. A single spectrograph will multiplex up to five nearest neighbor combinations onto a single detector. Identical spectrographs are located at opposite sides of the combiner outputs to simultaneously sample combination pairs that are π radians out of phase with respect to one another.

Keywords: MROI, interferometry, fringe tracking, baseline bootstrapping, pupil plane combination

1. INTRODUCTION

The "Y" configuration of the MROI[1] naturally lends itself to the baseline bootstrapping[2] technique for fringe tracking. Figure 1 is a simple schematic that illustrates the method. In the figure, telescope stations (represented by circles) are numbered 1 (inner), 2 (middle), and 3 (outer) within a given arm N (North), S (South), or W (West). Arrows represent the nearest neighbor combinations that are made to bootstrap the array from the outer to the inner telescopes in a given arm, and then from the inner telescopes through the central (W0), to phase up the three arms.

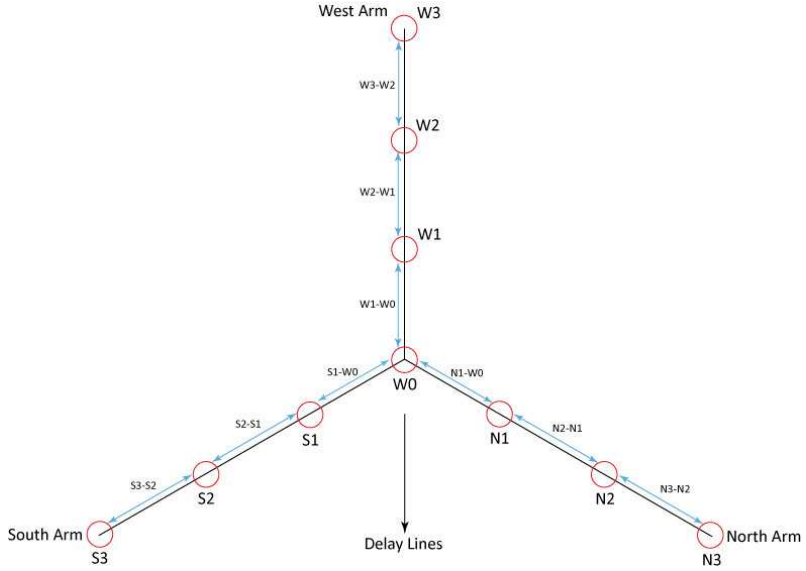

Fig. 1. Schematic illustrating the bootstrapping technique to be employed at the MROI. Telescope stations are represented by circles labeled 1 through 3, and the nearest neighbor combinations necessary to phase up the array are represented by the arrows connecting the stations.

1.1 Location in the Optical Train

There are a total of three beam combiners planned for the MROI. One each for visible science, IR science, and fringe tracking. Figure 2 locates the combiners in the array optical train. Upon exiting the delay lines, the beams enter the beam combining area (BCA) where they are directed toward the switchyards. Dichroics in the switchyards select the appropriate bandpasses to be sent to the corresponding combiners. Although both the IR science and fringe tracking combiners operate in H and K bands, they do not share light. If the science combiner receives light in the H band, the fringe tracker will operate at K, and vice versa. As can be seen in the figure, the fringe tracker table is third in line, following the visible and then IR science table.

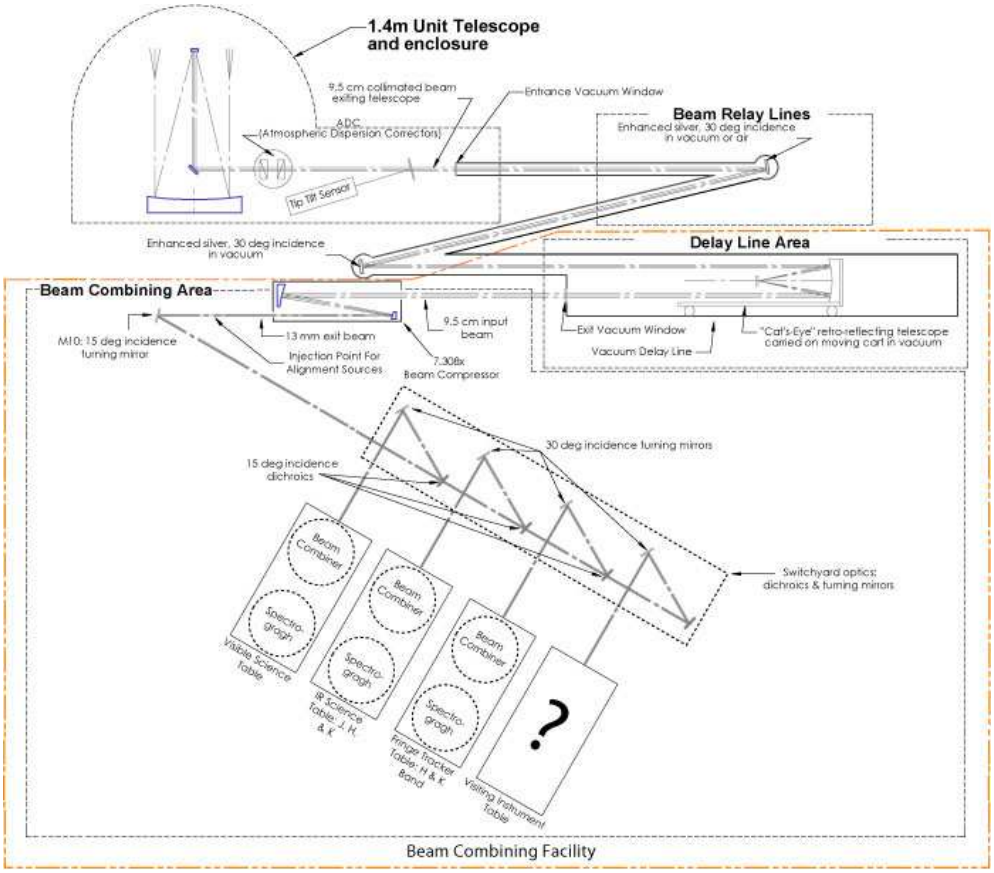

Fig. 2. The MROI optical train. Upon exiting the delay lines, beams travel into the BCA where different bandpasses are selected by the switchyards and sent to either a visible science combiner, an IR science combiner, or the fringe tracking combiner. The fringe tracker operates at either H or K_s, but does not take light away from the IR science combiner.

2. SYSTEM ARCHITECTURE

Figure 3 is an overview of how the system functions as an entity. In this simplified case light from three telescopes (N1/W0/S1) enters the combiner, and two pairs of outputs, π radians out of phase (e.g. N1-W0/W0-N1), enter the spectrograph. The spectrograph disperses the four fringe patterns into five spectral channels onto a detector. This constitutes the 0 and π measurements (A and C) in the A,B,C, and D modulation scheme. Once the four columns of five pixels are read out by the system "brain," it then instructs the beam combiner to modulate the input beams by $\pi/2$ radians to get the two remaining B and D measurements. The process of reading out the detector is then repeated, and the "brain" has enough information to determine the group delay which is used to calculate the delay offsets to be applied to the delay lines. In this case, bootstrapping is done through W0, so the offsets are only applied to N1 and S1.

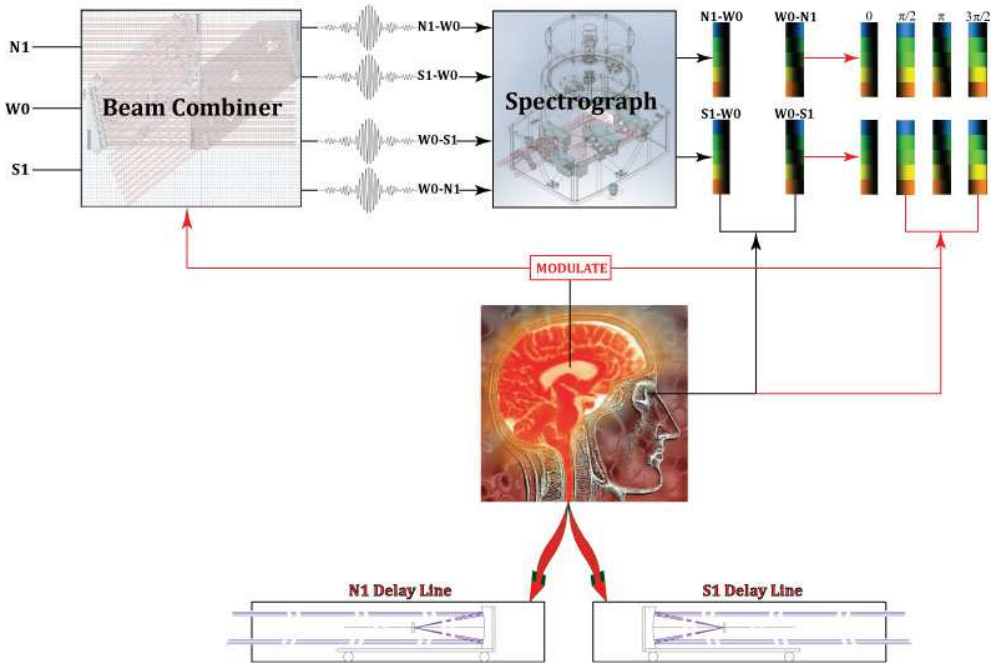

Fig. 3. Schematic illustrating the function of the fringe tracking system. In this case, light from three telescopes enters the combiner and four complimentary outputs are dispersed into 5 spectral channels by the spectrograph. After modulation, all four A, B, C, and D measurements have been made, and delay offsets are then applied to the N1 and S1 delay lines. In this case, bootstrapping is done through W0.

2.1 System components

The fringe tracker is composed of five subsystems that will be briefly outlined here, and discussed in more detail in the following sections. Four of these five subsystems are shown in Figure 4, and are the switchyard, beam combiner, dewar feed optics, and spectrograph. Not shown in the figure is the control system, or the "brain," which was briefly mentioned and discussed in relation to Figure 3. For scale, the two tables in Figure 4 are 2x4 meters.

Each of the main functions these subsystems perform are briefly listed here:

- Switchyard: configures the input phase plane to match that which the combiner is expecting as well as ensuring that combination partners arrive in the combination plane at the correct location, and traveling in the right direction.
- Beam Combiner: takes the inputs from the switchyard and makes the necessary nearest neighbor combinations to bootstrap the array.
- Dewar Feed Optics: folds the linear output pattern of the beam combiner into that of an arc so that multiple combiner outputs may be fed into a single dewar. These optics also ensure that light arrives at the pinholes inside the dewar at the correct location and traveling in the right direction.
- Spectrographs: disperses the combiner outputs into five spectral channels onto the detector.
- System Brain: reads out the detector and calculates the necessary offsets to be applied to the delay lines. It also controls all timing functions between the modulators and detector.

A key design feature of the combiner is that it is made without any internal degrees of freedom because it can be fabricated with enough precision to get light through it. The fine tuning alignment is done using the switchyard mirrors, to remove tilt and shear errors between combination partners in the combination plane. This is done using an optical arrangement at the combiner output to simultaneously measure tilt and shear. These components are illustrated in Figure 4 as well as part of the automated alignment system[3]. Although not directly part of the fringe tracker work package, they are an integral part of it.

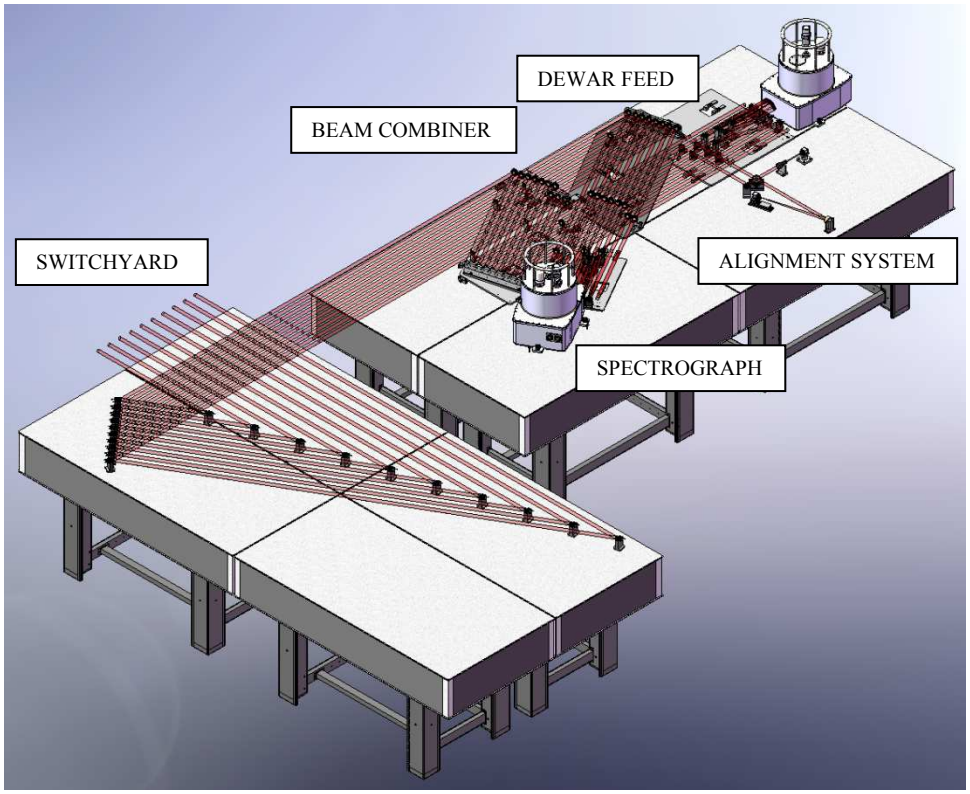

Fig. 4. The fringe tracker system components. It is made up of a total of five subsystems: 1. the switchyard, 2. beam combiner, 3. dewar feed optics, 4. spectrographs, and 5. system brain. Also included in the figure, but not part of the fringe tracker system are the automated alignment system components. The two tables are 2m x 4m in size.

3. THE SWITCHYARD: CONFIGURATOR OF THE PHASE PLANE

Referring back to Figure 2, the MROI optical train, the beams exit the delay lines before being reduced by the beam compressors. At the output of the beam compressors, they are redirected toward the switchyards by the M10 turning mirrors. Besides changing the direction of travel, the M10 turning mirrors also decrease the beam pitch from the delay lines, as well as change the phase plane.

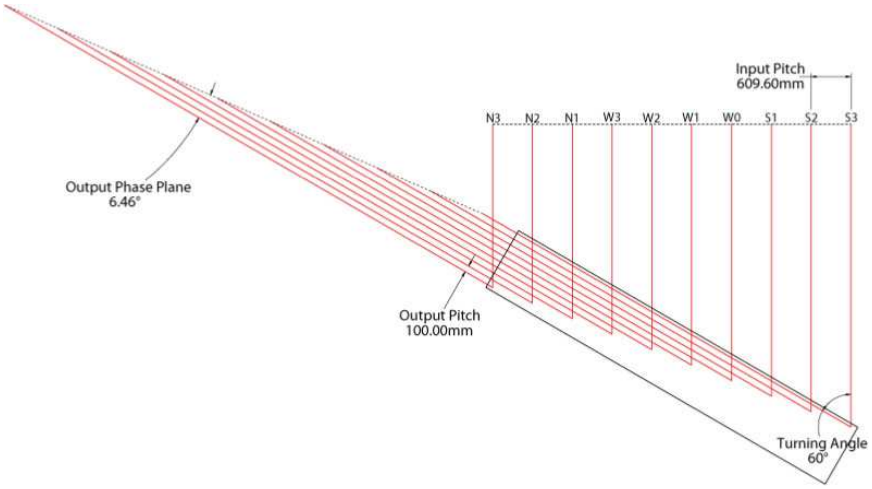

Fig. 5. Schematic of the M10 turning mirrors. Both beam pitch and phase plane are reconfigured.

Figure 5 is a two dimensional schematic of the M10 mirrors following the beam compressors. The input beams are labeled according to telescope locations in the array arms as in Figure 1. The input pitch from the delay lines is 609.6mm, while the input phase plane is perpendicular to the direction of travel (input and output represented by the dashed lines). From the figure, the beams are reflected through 60°, reducing the beam pitch to 100mm, and reconfiguring the phase plane to 83.54° normal to the direction of travel. The switchyard must therefore take the input beam pitch and phase plane following M10 and convert it to that which the fringe tracker beam combiner is expecting.

3.1 Switchyard Layout

A pair of turning mirrors with remotely adjustable tip/tilt actuation make up the switchyard. It is these mirrors that the alignment system uses to remove tilt and shear errors between combination partners in the beam combiner combination plane. These mirrors not only redirect the light by 90° while maintaining polarization purity, but they alter the beam pitch, reconfigure the plane of constant phase, and allow the beams to be switched while maintaining all of the afore mentioned factors. The input phase plane will be discussed in the next section on the beam combiner design. Figure 6 is a three dimensional, scaled drawing of the switchyard. The table size is 2x4 meters. In the figure, beams are input from the upper right, and are output at middle right.

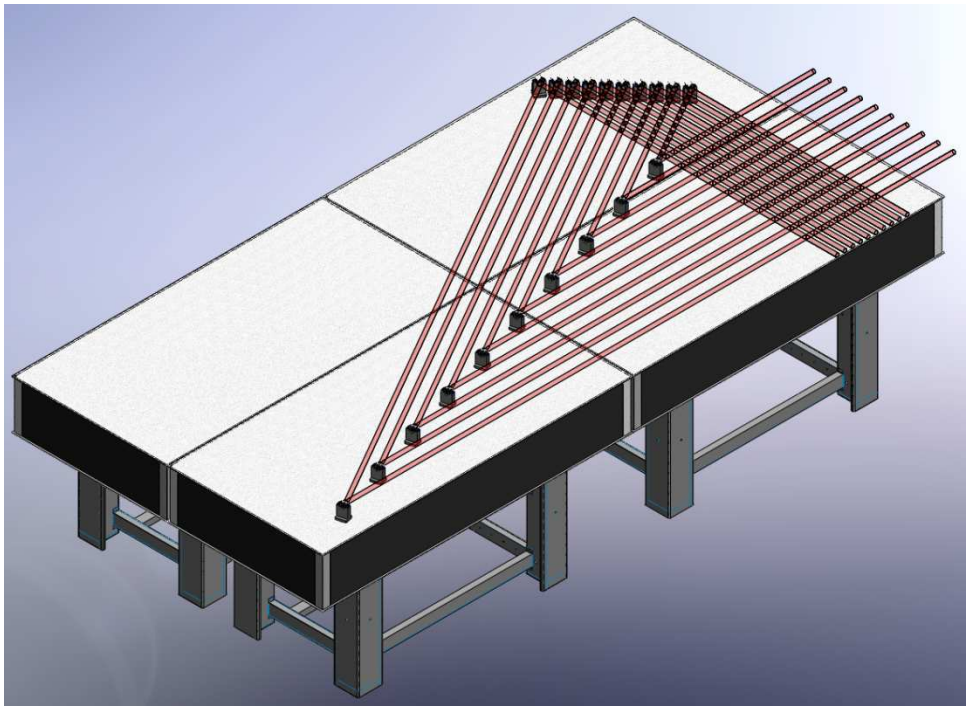

Fig. 5. CAD drawing of the switchyard optical layout. Input beams from M10 with 100mm spacing enter at upper right, while output beams with 50mm spacing are directed toward the middle right. For scale, the table is 2x4 meters.

4. COMBINER ARCHITECTURE - SYMETRY BREAKING IN THE TOPOLOGICAL LANDSCAPE

Given the topological layout of the array, a very specific beam combination scheme is needed to in order to baseline bootstrap (see Fig. 1). This is illustrated below in Figure 6. In the figure, beams enter from the upper left. The input phase plane from the switchyard is represented by the dashed line. Nearest neighbor complimentary outputs are labeled at lower left and right. Close inspection shows that all '3' telescopes have one combination partner, '1' and '2' telescopes have two combination partners, and the W0, or vertex telescope has three combination partners. This has lead to a design that is modular in its extent, so that it can operate whether the MROI is populated with two telescopes or ten, as will be discussed below. A detailed analysis of this combiner architecture[4] with theoretical coating performance shows that the combiner itself will not be a limiting factor in the performance of the instrument.

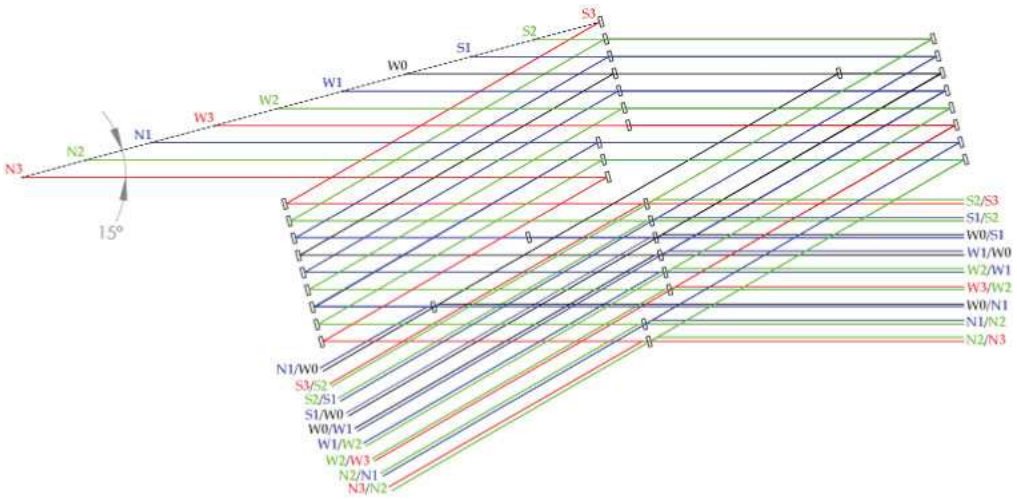

Fig. 6. Optical layout of the MROI fringe tracking beam combiner. Light from the telescopes enters from the switchyard at upper left, and the complimentary outputs are labeled at lower left and middle right. The switchyard inputs a phase plane illustrated by the dashed line. All '3' telescopes have one combination partner, '1' and '2' telescopes have two combination partners, and the W0 (vertex telescope) has three combination partners.

4.1 Modular Design Approach

The MROI is being built in two phases of operation: Phase A) six telescopes, IR science and fringe tracking combiners, and Phase B) ten telescopes with additional visible science combiner. Since the phases will take place over several years, it was determined to be necessary for the fringe tracking combiner design to accommodate the build-up of telescopes with minimal reconfiguration effort of the combiner itself. Figure 7 illustrates the first aspect of this approach.

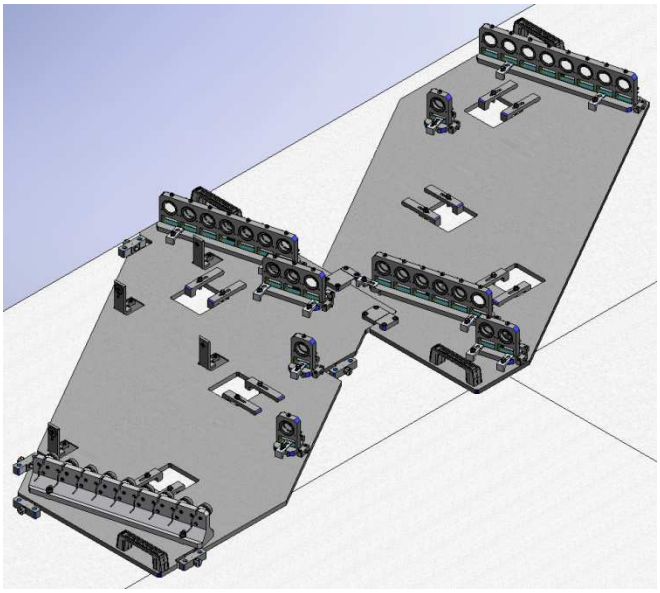

Fig. 7. Beam combiner alignment templates with optical mounts. The first template (lower left) is aligned on the table using reference beams from the delay lines, and the second template is aligned relative to it along two edges. The optical mounts on the templates are clamped to the templates with the correct spacing and orientation to within the fabrication tolerances of the plates themselves.

In the figure, two large alignment templates are oriented onto the optical table using reference beams from the delay lines. Optical mounts that house the beam combiner optics are clamped to the templates with the correct spacing and orientation to within the fabrication tolerances of the plates themselves. The templates are matched in CTE to the optical

table skins, and the optical mounts are constrained to expand and contract due to thermal variations in the same directions. The driving force behind this arrangement is that once the rough alignment is accomplished using the reference beams, the fine alignment can then be completed using the switchyard mirrors.

The optical mounts on the templates were designed to allow for interchanging of optics to maintain the nearest neighbor combinations for bootstrapping the array when operating with less than ten telescopes. This concept is illustrated in Figure 8. At left in the figure is an example of one of the mounts that contains three optical cells. Within each cell is placed an optic that fits within the overall beam combination scheme as illustrated in Figure 6 regardless of the number of telescopes. Figure 9 further explains the need for this flexibility.

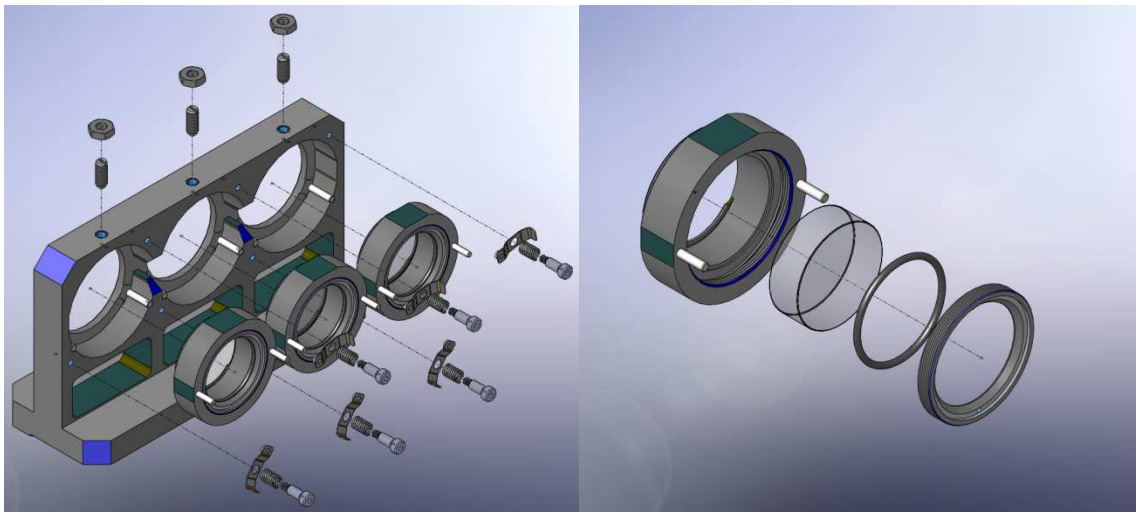

Fig. 8. *Left:* Example of a beam combiner optical mount that is clamped to the alignment templates. *Right:* Optical cell that is slid into place in the optical mounts. This arrangement allows for minimal reconfiguration of the beam combiner as the array phases up to ten telescopes. All that is required is for the appropriate optical cell to be placed in the proper location to maintain nearest neighbor combinations.

From Figure 6 it was determined that given this combiner architecture with a ten telescope array, all '3' telescopes have one combination partner, '1' and '2' telescopes have two combination partners, and W0 has three partners. When operating with less than ten, the roles of outer to inner telescopes shift. Figure 9 illustrates the case for a six telescope array that corresponds to the completion of Phase A. At left, the array is populated with two telescopes in the south and west arms, and one in both the center and north arm. The illustration at right is the corresponding combiner layout. As can be seen through comparison with Figure 6, the '2' telescopes in the west and south arms now take the role of a '3' telescope as does the '1' telescope in the north arm.

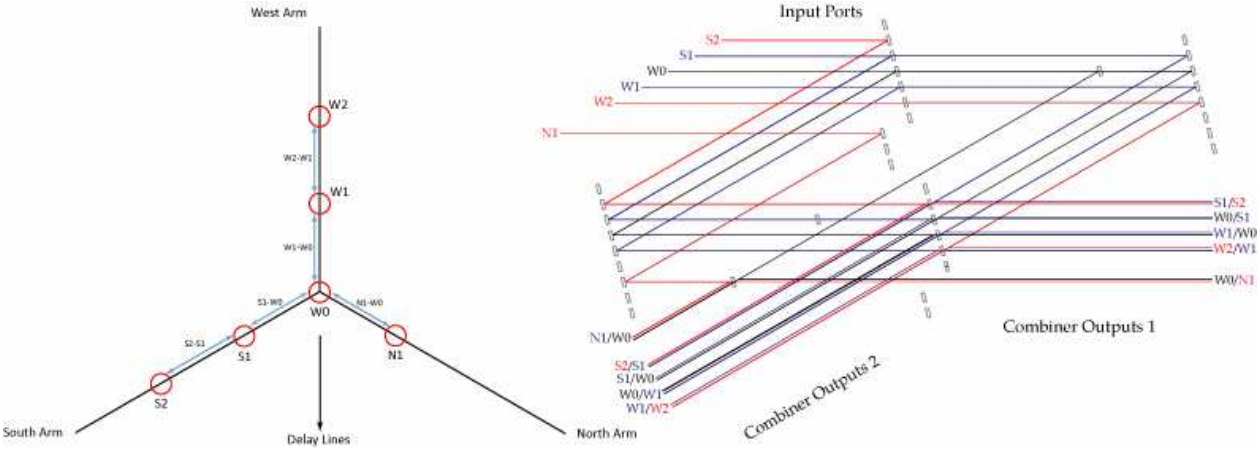

Fig. 9. *Left:* Array populated with six telescopes. *Right:* Corresponding beam combiner layout to maintain nearest neighbor combinations for bootstrapping.

4.2 OPD Modulation Strategy

As was discussed in Section 2 on system architecture, it is optics within the beam combiner that performs modulation to get the needed A, B, C, and D measurements. For this combiner architecture, for X input beams, a non-redundant X-1 of them must be modulated. This prerequisite is met by a single bank of mirrors within the combiner, and its location is highlighted in Figure 10. In the figure, input beams are shown entering the combiner at lower left, and the two outputs at upper right and lower middle. The bank of modulator mirrors is labeled at lower left.

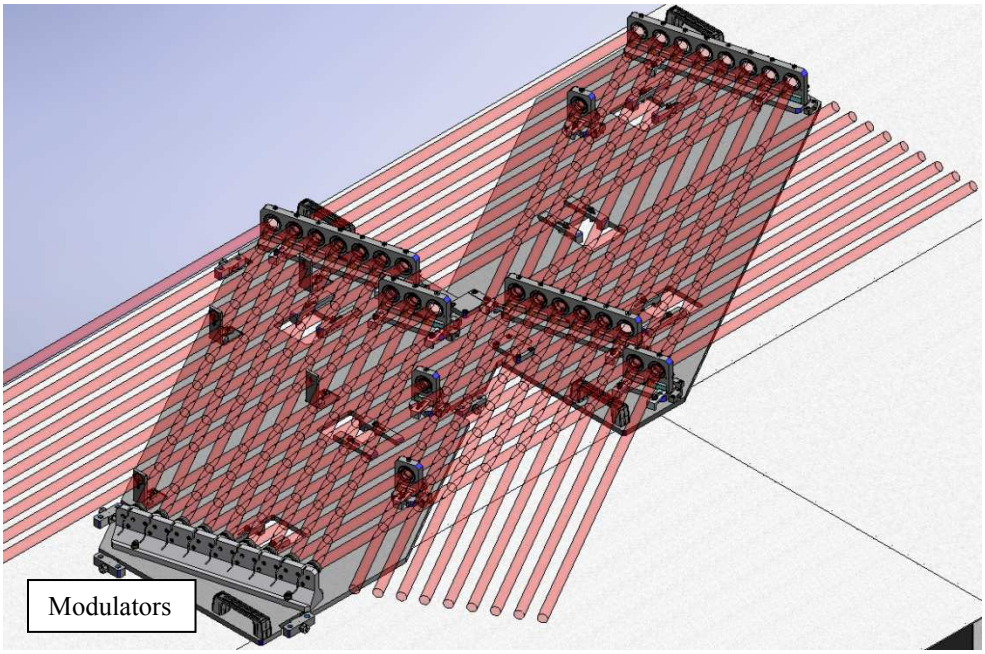

Fig. 10. Beam combiner layout with beams highlighting the location of the modulator mirrors within the combiner. For this combiner architecture, with X input beams, a non-redundant X-1 must be modulated. This prerequisite is met by the bank of mirrors labeled above.

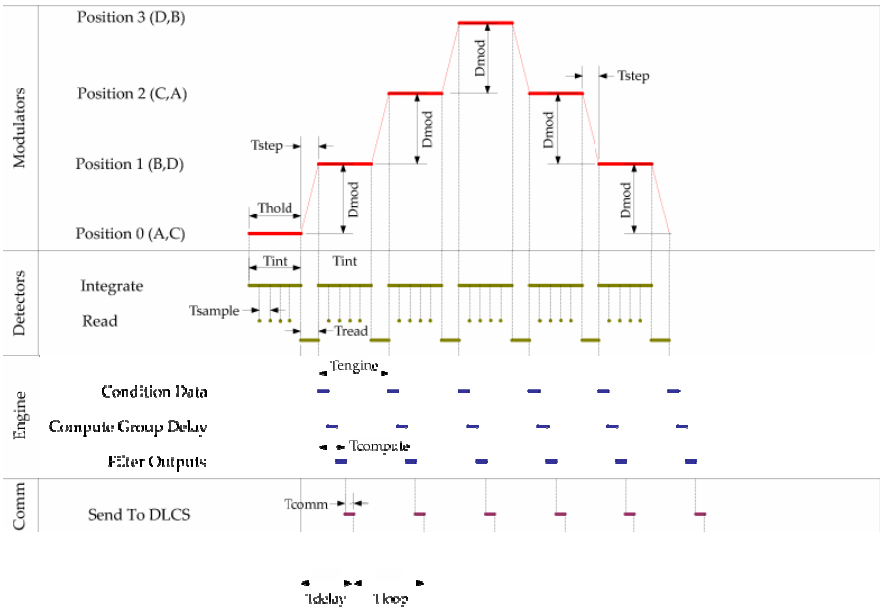

Fig. 11. OPD modulation timing sequence and waveform. In the scheme illustrated here, the modulator is stepped by $\pi/2$ radians in two directions to obtain the A, B, C, D measurements. The time between steps is variable and dependent upon source brightness and atmospheric conditions.

There are two waveforms that can be employed for the modulation scheme, a sawtoothe and a step pyramid, however, the step pyramid is the primary and will be the only one discussed here. It consists of stepping the modulators in three positions separated by $\pi/2$ radians at a chosen wavelength in the bandpass. This is illustrated in Figure 11. At Position 0, A and C are sampled at the two combiner outputs. The position is held (T_{hold}) while the detector integrates (T_{int}) and is sampled nondestructively a predetermined number of times (T_{int}/T_{sample}). The modulator is then stepped to Position 1 to get the B and D measurements and the read process is repeated.

At this point the modulator is now moved in the same direction to Position 2 where A and C are sampled again, but on different detectors from Position 0. Once the reading process is complete, the modulator is stepped to Position 3 and B and D are sampled on different detectors, as was the case for A and C at Position 2. The modulators then step back in the direction they came repeating the process. The point of this modulation scheme is to ensure that the A, B, C, D parameters are all sampled on both detectors, and in both directions of the modulator travel. Therefore any systematic errors due to differences in the detectors or modulator travel can be accounted for.

In the figure, T_{step} is the time between modulator position moves, and will be variable depending upon source brightness and atmospheric conditions. At its fastest, it will operate at 200Hz, and depending upon the algorithm being employed (see Section 7) offsets can be sent back to the delay lines after each step (using a running average), after two (obtaining all four samples), or some integer number of either these two options. These are all being explored in the algorithm/simulator development.

5. DEWAR FEED OPTICS

The dewar feed optics serve two main functions:

1. Take the linear output pattern of the combiner and fold it into an arc.
2. Ensure that the beams arrive at the dewar pinholes at the correct location, traveling in the right direction.

The first function is the allows for five nearest neighbor combinations to be multiplexed onto a single detector at each output. This therefore requires two dewars (one at each combiner output) for Phase A development of the interferometer. During Phase A, the array will have up to six telescopes, resulting in ten combinations, five at each output. Once the MROI transitions into Phase B with the arrival of the seventh telescope, another set of dewars will be required. All four however will be identical, the only difference between the Phase A and Phase B dewars is the number of combiner outputs they need to accommodate (5 and 4 respectively).

Function number two listed above is the alignment mechanism for each combiner output, serving a similar role as that defined for the switchyard. As was discussed in Section 3, the pair of switchyard optics remove tilt and shear errors between combination partners in the combination plane. It was also mentioned that these optics accomplish the fine alignment of the beam combiner itself. Similarly, the dewar feed optics ensure each combiner output arrives at its dewar pinhole at the correct location and traveling in the right direction.

5.1 Opto-mechanical Layout

Much like the beam combiner alignments, the dewar feed optics have their own as well. From the image at left in Figure 12, they mate along two edges of the beam combiner alignment templates, which were previously aligned to the delay line reference beams. This provides the initial rough alignment, with the pair of mirrors for each combiner output providing the fine alignment as discussed above.

In the left figure, the set of optics at upper left (projection mirrors) are the first set of optics that are placed at the outputs of the beam combiner, and then project the beams into the arc configuration mirrors shown in the middle. There are a total of nine projection mirror stations, with ten telescopes they will all be filled. Shown here is Phase A operation of six telescopes (five stations). The azimuth angle of both projection and arc mirrors can be configured depending upon beam combiner output location. Top right in the figure shows the formation of the arc in elevation, and bottom right looks into the arc configuration mirrors from the perspective of the dewar windows.

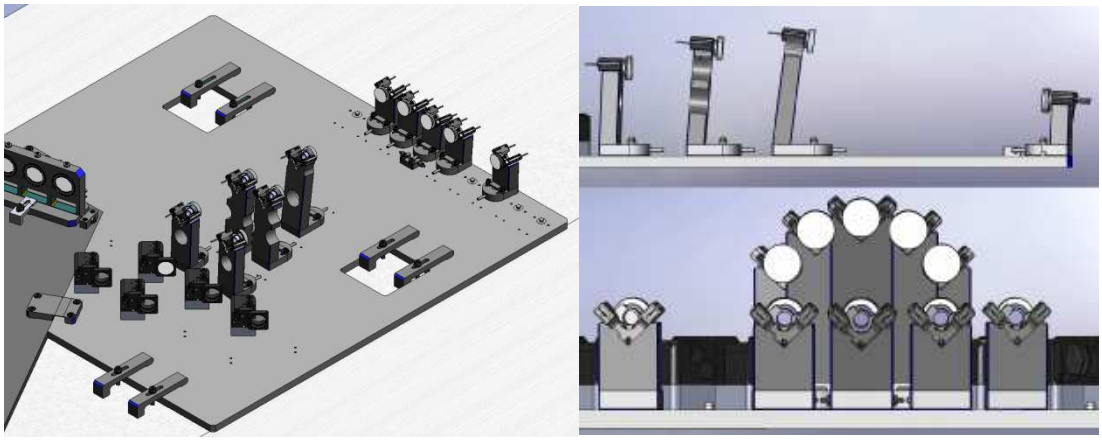

Fig. 12. *Left:* Highlights the use of the alignment template for the dewar feed optics as well as the use of projection and arc mirrors to feed the spectrographs. *Right Top:* Shows the formation of the arc in elevation, and *Right Bottom:* Looks into the arc mirrors from the perspective of the dewar windows.

6. SPECTROGRAPH DESIGN

For Phase A operation of the MROI, two spectrographs are needed, one at each combiner output, accommodating up to five nearest neighbor combination inputs. For Phase B, another two spectrographs will need to be built to collect all nine combiner outputs. The opto-mechanical design is identical in all four cases, the only difference being the number of inputs received from the combiner.

6.1 Optical Layout

Figure 13 is a three dimensional isometric view of the optical layout illustrating the optical components that reside in the dewar. The beams are input in an arc pattern from the dewar feed optics, and are then filtered in either H or K_s Band. Following the filters, they are focused down through a set of pinholes by five pairs of off axis parabolae (OAPs) in an Eccentric Mersenne Gregorian (EMG) configuration. Upon recollimation the beams are then dispersed by a set of Direct View Prisms (DVPs) before being focused onto the detector into five spectral channels.

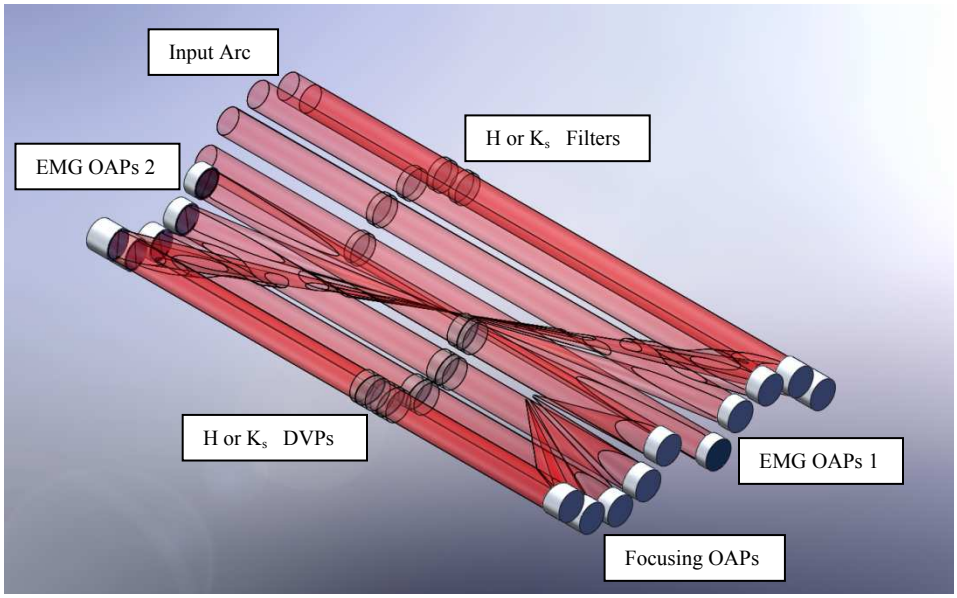

Fig. 13. Optical layout of the spectrograph. Beams enter from the dewar feed optics in an arc pattern, are filtered, focused down through a set of pinholes, recollimated, dispersed, and then focused onto the detector into five spectral channels.

The primary dispersing element of the DVPs is $SrTiO_3$, while ZnS[5] acts to bend the rays back towards the original optical axis. In the left hand side of Figure 13, the DVP optical cell is shown with the two elements. Separate sets have been designed for both H and K_s bands, so that the dispersion takes place over the same five pixels. At right in the figure shows the dispersed spot diagrams for K_s band, in the pattern of an arc, as it would appear on the detector. Illustrated at right upper middle is the worst case aberrated spot in either band (2.31 μm). The circle represents the Airy disk, contained within a pixel for the PICNIC array. This optical configuration will provide diffraction limited performance across both bands.

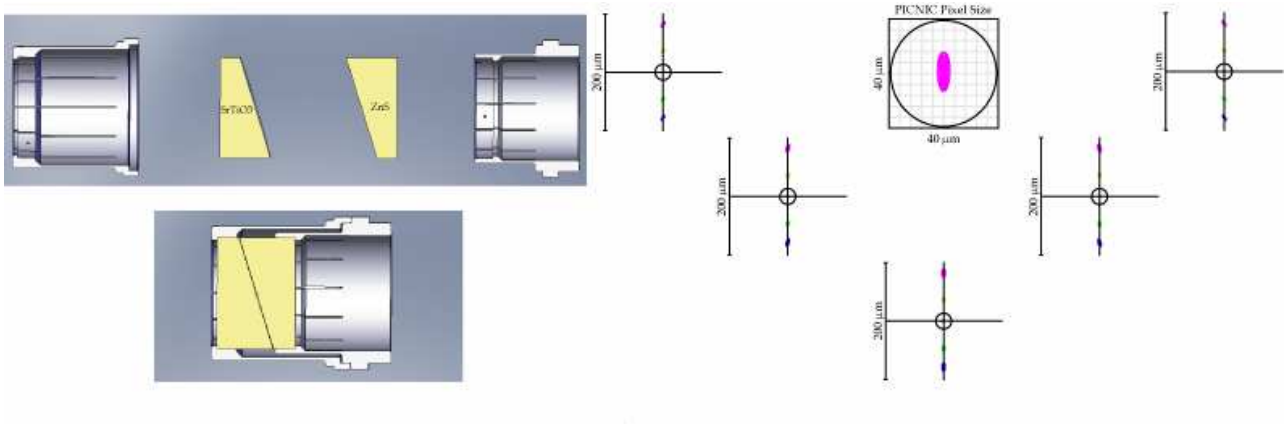

Fig. 14. *Leftt:* The DVP cell assembly with the dispersing elements SrTiO3 and ZnS. *Right:* Dispersed Spot diagrams in Ks band in the pattern of an arc as they would appear on the detector.

6.2 Dewar Design Features

The dewar design is shown in figure 15. At left, the dewar windows in the pattern of an arc can be seen at lower left corner of the image. The shell has been made transparent, illustrating the LN_2 tank contacted to the optics baseplate via copper braids. Also shown are two of the four bi-pod flexures that connect the optics baseplate to the dewar plate. These flexures not only ensure a stable platform for the optics, but have a low thermal conductivity.

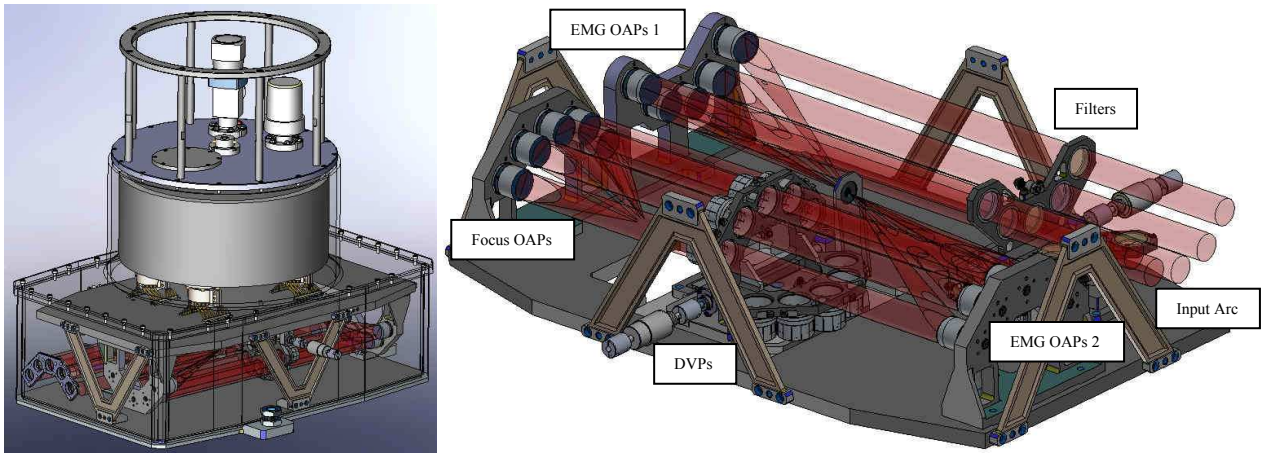

Fig. 15. *Left:* The dewar with the outer shell transparent highlighting its design features. The arc input pattern of the dewar windows can be seen at lower left. *Right:* Dewar baseplate inverted to show mounted optical components from Figure 13.

At right in Figure 15 shows the optics baseplate, inverted, to highlight the optical mounts. All four bi-pod flexures are also seen (inverted 'V' along edges of plate). The baseplate, curved optics, and all mounts will be constructed from the same aluminum alloy. Instead of traditional motorized wheels for the filters and DVPs, the MROI engineers have designed a flipper "butterfly" mount that accommodates the space constraints of the dewar, as well as the arc pattern of the beams. For scale, the baseplate is 500mm in length, and 275mm in width.

7. ALGORITHM DEVELOPMENT

In parallel with the opto-mechanical design being done at MRO, the University of Cambridge is developing a simulator to aide in the development of the fringe tracking algorithms. The purpose of the simulator is to model the performance of fringe tracking at the MROI, particularly how this performance varies with the SNR of the target being observed. It will also be used to evaluate fringe acquisition and tracking algorithms for cophasing and coherencing modes, as well as the bootstrapping strategy.

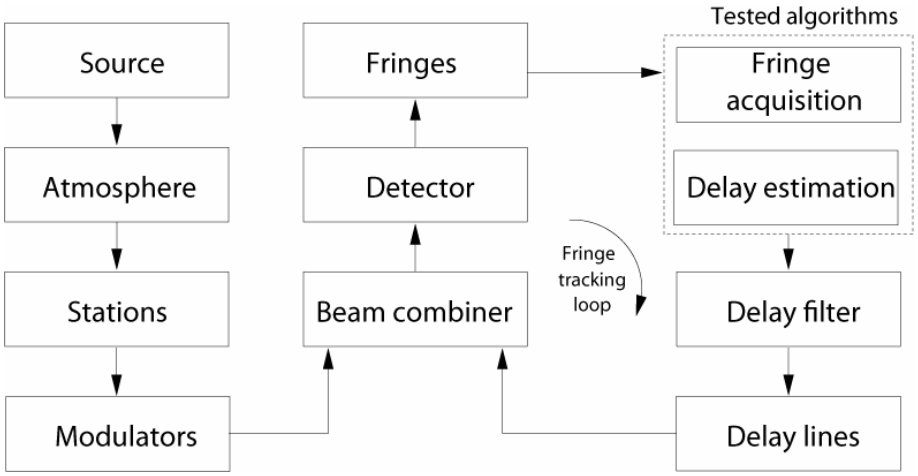

Fig. 16. Software architecture used for the fringe tracker simulator to aide algorithm development.

The software architecture of the simulator is shown on Figure 16. Several interrelated modules will simulate in pseudo-real-time the diverse components of the fringe tracking loop. The simulation includes atmospheric perturbations, source spatial and spectral frequencies, actual station positions, modulator and delay line mechanical responses, and the noisy detection process. The program will be event-based, allowing it to simulate simultaneous events, and take into account relevant time delays such as the data transmission or the data processing delays. The fringe tracking algorithms will include classic cophasing and coherencing algorithms, as well as predictive ones[6,7,8,9].

REFERENCES

[1] Creech-Eakman et al., "Magdalena Ridge Observatory Interferometer: progress towards first light," Proc. SPIE 7013, 2008.

[2] Armstrong, J.T., Mozurkewich, D., Pauls, T.A., Hajian, A.R., "Bootstrapping the NPOI: keeping long baselines in phase by tracking fringes on short baselines," Proc. SPIE 3350, 461-466, 1998.

[3] Shtromberg, A.V., Jurgenson, C.A., Paz, T., Steenson, J., Berger, L., "MROI's Automated Alignment System," Proc. SPIE 7013, 2008.

[4] Block, E.K., Jurgenson, C.A., Buscher, D.F., Haniff, C.A., Young, J.S., Creech-Eakman, M.J., Jaramillo, A., Schmell, R., "The Magdalena Ridge Observatory Interferometer: Custom Near-IR Beamsplitter and AR Coatings," Proc. SPIE 7013, 2008.

[5] Takato, N., Terada, H., "Near-Infrared Direct Vision Prism for Wide-Wavelength Coverage Spectroscopy at the Subaru Telescope," Proc. SPIE 6269, 6269-23, 2006.

[6] Pedretti, E., Traub, W.A., Monnier, J.D., Millan-Gabet, R., Carleton, N.P., Schloerb, P.T., Brewer, M.K., Berger, J.P., Lacasse, M.G., Ragland, S., "Robust determination of optical path difference: fringe tracking at the Infrared Optical Telescope Array interferometer," Applied Optics, vol. 44, Issue 25, pp. 5173-5179.

[7] Thureau, N.D., Boysen, R.C., Buscher, D.F., Haniff, C.A., Pedretti, E., Warner, P.J., Young, J.S., "Fringe Envelope Tracking at COAST," Proc. SPIE 4838, 965, 2003.

[8] Morel, S., Traub, W.A., Bregman, J.D., Mah, R.W., Wilson, E., "Fringe-tracking experiments at the IOTA interferometer," Proc. SPIE 4006, 506, 2000.

[9] Padilla, C.E., Karlov, V.I., Li, J., Chun, H.M., Tsitsiklis, J.N., Reasenberg, R.D., Proc. SPIE 2477, 63, 1995.